Polymer Chemistry

Accepted Manuscript

ROYAL SOCIETY OF CHEMISTRY

www.rsc.org/polymers

Journal Name

RSCPublishing

COMMUNICATION

Thiol-reactive Passerini-methacrylates and Polymorphic Surface Functional Soft Matter Nanoparticles via Ethanolic RAFT Dispersion Polymerization and Post-synthesis Modification

Cite this: DOI: 10.1039/x0xx00000x

Received ooth January 2012,
Accepted ooth January 2012

DOI: 10.1039/x0xx00000x

www.rsc.org/

Yiwen Pei,[a,b] Janina-Miriam Noy,[a] Peter J. Roth[a]* and Andrew B. Lowe[a,b]*

RAFT dispersion polymerization (RAFTDP) is used to prepare reactive nanoparticles via the incorporation of Passerini-derived methacrylic comonomers containing pentafluorophenyl (PFP) groups. Copolymerization of 2-(dimethylamino)ethyl methacrylate with a Passerini comonomer gives copolymers suitable as macro-CTAs for ethanolic RAFTDP of 3-phenylpropyl methacrylate. Reaction of the PFP residues with functional thiols offers an approach for preparing surface modified nanoparticles.

Reversible addition-fragmentation chain transfer dispersion polymerization (RAFTDP) has recently attracted attention as a convenient one-pot process for preparing soft matter nanoparticles exhibiting diverse polymorphism.[1-3] There is now a large volume of literature detailing various RAFTDP formulations with the majority describing syntheses in alcoholic[4-6] or aqueous media,[3] plus several examples in non-polar solvents.[7, 8] While a versatile and straightforward process, there is one aspect that has yet to be fully exploited, namely the preparation of particles containing reactive handles, ideally in the solvophilic shells, that are amenable to chemical modification. Examples of such desirable species include pentafluorophenyl esters[9, 10] and azlactone-containing[5, 11, 12] species. Unfortunately, there is a fundamental incompatibility of these key functional groups with common RAFTDP formulations. For example, both these species are sensitive towards OH-containing molecules at ambient or elevated temperature and will be consumed during RAFTDP in common polar media if incorporated into the stabilizing macro-CTA or core-forming blocks.

Given the versatility associated with such reactive handles, it is desirable to establish an approach for the incorporation of such species, or closely related functionality, in RAFTDP systems. Herein we report a viable approach for the introduction of thiol-reactive species in the coronae of nanoparticles prepared via alcoholic RAFTDP. Key to the approach is the use of novel pentafluorophenyl (PFP)-containing methacrylic monomers prepared via the Passerini reaction[13-16] as described recently by Roth et al.[17, 18] The overall approach is shown in Scheme 1.

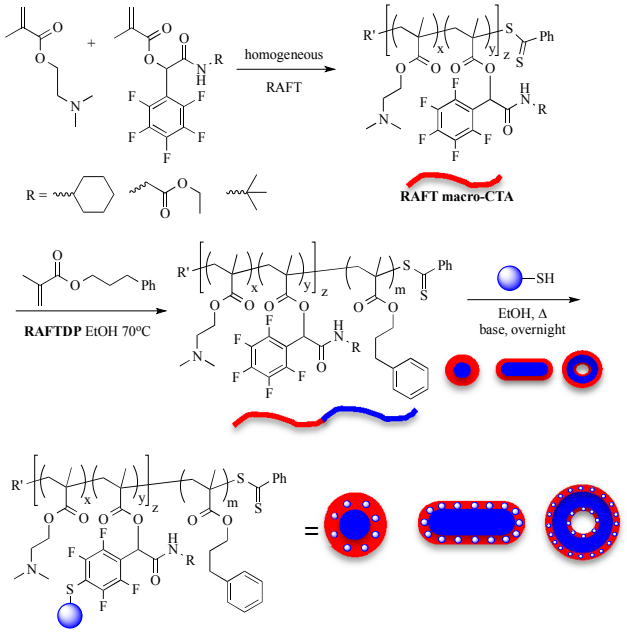

Scheme 1. The synthesis of surface-functional polymeric nanoparticles via a combination of homogeneous RAFT with Passerini-synthesized methacrylates (R = cyclohexyl = 2-(cyclohexylamino)-2-oxo-1-(perfluorophenyl)ethyl methacrylate (CyAFPEMA); R = ethylester = 2-((2-ethoxy-2-oxoethyl)amino)-2-oxo-1-(perfluorophenyl) ethyl methacrylate (EAFPEMA) or R = *t*-butyl = 2-(*tert*-butylamino)-2-oxo-1-(perfluorophenyl)ethyl methacrylate (*t*BAFPEMA)), RAFT dispersion polymerization and nucleophilic aromatic substitution with thiols.

Homogeneous RAFT copolymerization of 2-(dimethylamino)ethyl methacrylate (DMAEMA) with a small amount of a Passerini comonomer (CyAFPEMA, EAFPEMA or *t*BAFPEMA) for an overall target average degree of polymerization ($\bar{X}_n$) varying from 31 to 38, performed in MeCN, yielded the parent macro-CTAs, Table 1. Conversions were intentionally limited to maintain end-group fidelity, and this approach gave macro-CTAs with low dispersities ($Đ_M = \bar{M}_w/\bar{M}_n$), absolute molecular weights (as measured by ^{1}H NMR) up to ca. 7,000, with molar contents of Passerini comonomer of ca. 5 %, see SI. The macro-CTAs were subsequently employed in the ethanolic RAFTDP of 3-phenylpropyl methacrylate (PPMA) following our recently reported method, Table 2.[5]

Table 1. Summary of the compositions, molecular weights and dispersities ($Đ_M$) of the DMAEMA-Passerini RAFT macro-CTAs.

Macro-CTA	Conv. (%)	NMR molecular weight	SEC $\bar{M}_n$	SEC $Đ_M$
P(DMAEMA$_{36}$-*co*-CyAFPEMA$_2$) (**1**)	55	6,700	6,800	1.14
P(DMAEMA$_{29}$-*co*-EAFPEMA$_2$) (**2**)	52	5,300	6,600	1.16
P(DMAEMA$_{31}$-*co*-*t*BAFPEMA$_2$) (**3**)	55	5,900	6,400	1.16

Table 2. Summary of RAFTDP syntheses with macro-CTAs **1**-**3** and PPMA as comonomer in EtOH at 21 wt% and 70 °C. The NMR-determined average degree of polymerization ($\bar{X}_n$) of the PPMA block and absolute molecular weight are given along with the SEC-measured $\bar{M}_n$ and dispersities, TEM morphology and DLS-measured hydrodynamic diameters and polydispersities.

CTA	PPMA $\bar{X}_n$	NMR MW[a]	SEC $\bar{M}_n$[b]	SEC $Đ_M$[b]	TEM morp.[c]	DLS D_h[d]	DLS PDI
1	148	46,900	26,400	1.19	S+W	141.8	0.21
2	44	14,300	17,300	1.19	S	53.4	0.17
2	79	21,400	21,200	1.19	S+W	81.4	0.17
2	91	23,900	22,900	1.24	W+V	215.0	0.21
3	48	15,700	16,200	1.18	S	45.8	0.18
3	80	22,300	19,600	1.23	S+W	137.1	0.19
3	87	23,700	19,900	1.21	S+W	190.1	0.19
3	95	25,200	21,300	1.23	W	223.4	0.19
3	131	32,700	25,800	1.21	W+V	230.7	0.79

a. As determined by end group analysis; b. measured in THF on a system calibrated with polystyrene standards; c. S = spheres, W = worms, V = vesicles; d. hydrodynamic diameter in nm.

All RAFTDPs yielded soft matter nanoparticles presenting the full range of common morphologies. Fig 1 shows representative TEM images of the nanoobjects obtained in the RAFTDP of PPMA with macro-CTA **3**. For an $\bar{X}_n$ of the PPMA block of 48, Fig 1A, a pure spherical phase was observed while at an $\bar{X}_n$ of 87 a mixed phase was formed consisting of spheres and worms, Fig 1B. The diameter of the worm species is the same as the spheres and consistent with their formation via 1D coalescence of the spherical species. Increasing the PPMA block length by an average of 8 repeat units to 95 gives a pure worm phase, Fig 1C. In the most asymmetric species, with a PPMA $\bar{X}_n$ of 131, another mixed phase is observed comprised of worms and vesicles. The approximate sizes of all the nanoparticles, as measured by TEM, is consistent with values obtained by dynamic light scattering (DLS), see SI. Differences between DLS and TEM measured sizes are common and are due to the solution vs solid state nature of the measurements. Similar results were obtained with **1** and **2** and their RAFTDP with PPMA, see SI.

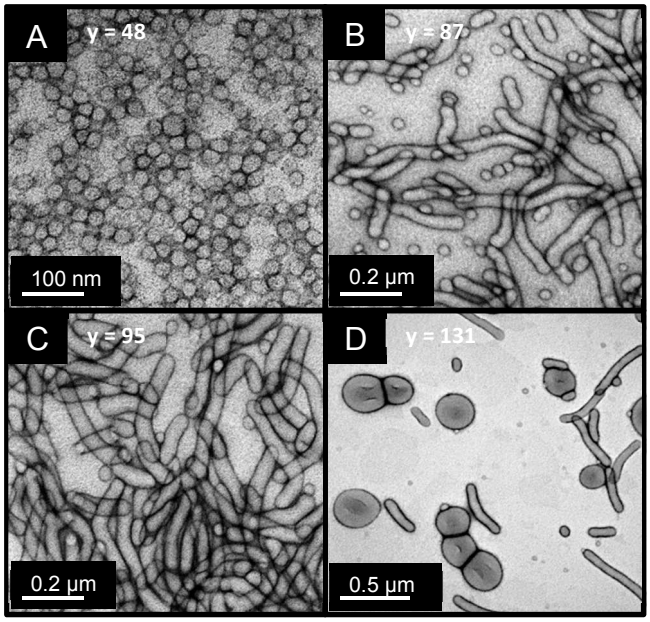

Figure 1. Representative TEM images of nanoparticles obtained from the RAFTDP of PPMA with the p(DMAEMA$_{31}$-*co*-*t*BAFPEMA$_2$) macro-CTA in EtOH at 70 °C for variable lengths of the PPMA block, y.

While the RAFTDP features of these Passerini-based copolymers is clearly of fundamental interest, the *primary* aim of this disclosure is to demonstrate how these polymeric nanoparticles, with Passerini species in the solvophilic blocks, can act as reactive scaffolds for the generation of new functional nanoobjects. Following particle syntheses, the PFP functionality associated with the Passerini units were reacted with thiols, in the presence of an organobase, at 50 °C in EtOH, in nucleophilic *para*-aromatic substitution reactions, Scheme 1. Spherical nanoobjects formed by p[(DMAEMA$_{31}$-*co*-*t*BAFPEMA$_2$)-*b*-PPMA$_{48}$] were reacted with 2-mercaptoethanol, 1-thio-β-D-glucose tetraacetate and cysteamine hydrochloride employing a 5-20 fold excess of thiol to PFP residues, while the pure worm phase nanoparticles obtained for p[(DMAEMA$_{31}$-*co*-*t*BAFPEMA$_2$)-*b*-PPMA$_{95}$] were reacted with 50 equivalents of the thiosugar in the presence of TEA. Also, the mixed S+W phase formed by p[(DMAEMA$_{31}$-*co*-*t*BAFPEMA$_2$)-*b*-PPMA$_{80}$] was reacted with captopril and thiophenol with a 5-10 fold excess of thiol to PFP. The products were characterized via a combination of ^{1}H/^{19}F

NMR, FTIR, SEC, DLS and TEM to evaluate the structure, molecular weight distributions, size, and morphology after modification. Most reactions with the p[(DMAEMA$_{29}$-*co*-EAFPEMA$_2$)-*b*-PPMA$_{44}$] or p[(DMAEMA$_{31}$-*co*-*t*BAFPEMA$_2$)-*b*-PPMA$_{48}$] spheres and p[(DMAEMA$_{31}$-*co*-*t*BAFPEMA$_2$)-*b*-PPMA$_{80}$] S+W nanoobjects resulted in quantitative substitution and formation of the thioether derivatives (the exception being cysteamine hydrochloride which also resulted in amide formation as judged by FTIR, see SI). As an example, Figure 2 shows the ^{19}F NMR of the parent macro-CTA 3, a block copolymer with PPMA and the product obtained from the reaction of the nanoparticles with the thiosugar.

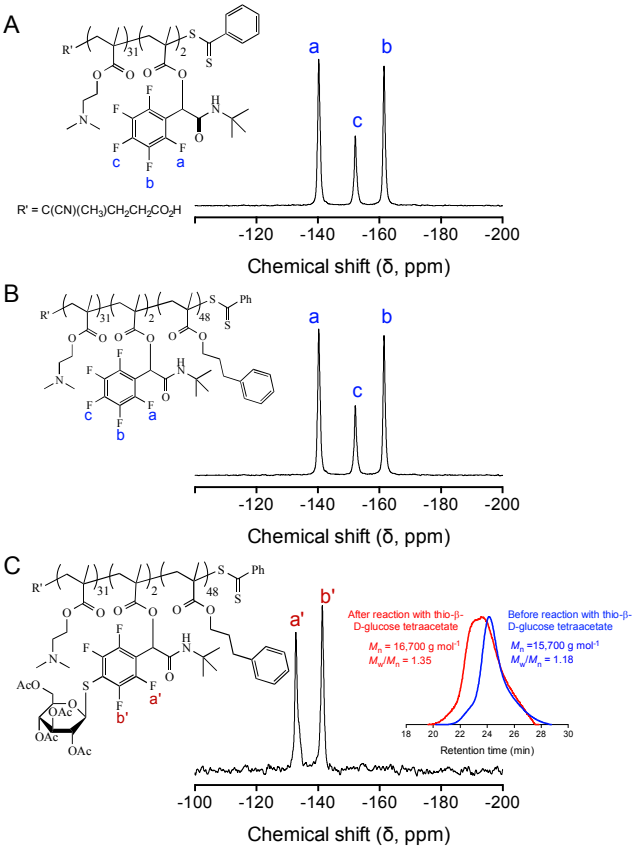

Figure 2. (A) ^{19}F NMR of the p[(DMAEMA$_{31}$-*co*-*t*BAFPEMA$_2$)] macro-CTA exhibiting *ortho*, *meta* and *para* signals associated with the PFP group in the Passerini repeat units; (B) after RAFTDP chain extension of 2 with PPMA showing the same distinctive pattern, and (C) after reaction of the spherical nanoparticles with thio-β-D-glucose tetraacetate, with SEC traces before and after reaction shown inset.

In the case of the macro-CTA **3** and the p[(DMAEMA$_{31}$-*co*-*t*BAFPEMA$_2$)-*b*-PPMA$_{48}$] copolymer, the ^{19}F NMR showed the expected signals associated with the *o*- (δ = -140.3 ppm), *m*- (δ = -161.8 ppm) and *p*- (δ = -152.4 ppm) fluorine substitution pattern of the Passerini monomer and confirmed the stability of these functional species under ethanolic RAFTDP conditions. After reaction with the thiosugar two differences are evident: i) only two resonances are seen with the signal associated with the *p*-fluoro group absent, and ii) the signal associated with the *m*-fluoro groups shifted by ca. 30 ppm from δ = -161.8 to -132.3 ppm. Both these features confirmed the quantitative reaction of the *p*-fluoro substituent and formation of the thioether glycopolymer nanoparticles. Similar observations were made for reactions conducted with other thiols, the exception being cysteamine hydrochloride, which resulted in some degree of amidation, see SI. In the case of modification of p[(DMAEMA$_{31}$-*co*-*t*BAFPEMA$_2$)-*b*-PPMA$_{95}$] worm nanoparticles with the thiosugar, ^{19}F NMR indicated near quantitative formation of sugar functional nanoparticles although some *p*-fluoro species were still present, see SI. Fig 2C also shows SEC traces of the p[(DMAEMA$_{31}$-*co*-*t*BAFPEMA$_2$)-*b*-PPMA$_{48}$] copolymer before and after modification with the thiosugar. The $\bar{M}_n$ increased, as expected, and the dispersity increased from 1.18 to 1.35 suggesting that the modification reaction is may be associated with some undesirable side reactions although this was not evident from the ^{19}F NMR or FTIR which qualitatively confirmed the absence of any undesirable side reactions (transesterification or thioester formation), except in the case of cysteamine hydrochloride where competing amidation was observed to occur, see SI.

Having shown that modification of the Passerini repeat units in the nanoparticle coronae proceeds (near) quantitatively without any effect on the molecular weight distribution of the parent (co)polymer we next examined the impact of the modification reaction on the parent particle morphology. Fig 3 shows TEM images and DLS-measured size distributions before and after modification of p[(DMAEMA$_{31}$-*co*-*t*BAFPEMA$_2$)-*b*-PPMA$_{48}$] and the worm-forming species p[(DMAEMA$_{31}$-*co*-*t*BAFPEMA$_2$)-*b*-PPMA$_{95}$] with the thiosugar. In the case of the p[(DMAEM$_{31}$-*co*-*t*BAFPEMA$_2$)-*b*-PPMA$_{48}$] spherical nanoparticles, TEM indicated no change in the morphology (Fig 3a and 3b). In fact, the DLS-measured D_h increased from ca. 45 to 70 nm while the polydispersity remained the same after modification (Fig 3e). In the case of the worm nanoparticles formed from p[(DMAEMA$_{31}$-*co*-*t*BAFPEMA$_2$)-*b*-PPMA$_{95}$], reaction with the thiosugar did result in a change in the observed morphology. The parent worm nanoparticles transformed into a mixed phase consisting of spheres and worms, Fig 3c and 3d. This result does not preclude the ability to modify worm nanoparticles without a change in morphology but more likely is a consequence of the rather specific conditions under which worm nanoparticles are commonly formed in RAFTDP. Armes et al.,[19-21] for example, has reported phase diagrams for various RAFTDP systems with a common feature being the narrow range of conditions under which pure worm phases are obtained. Since nanoparticle morphology is determined by numerous structural features, and often rationalized in terms of the packing parameter, *p* (a purely geometric approach to predicting morphology), it is likely that the post-polymerization incorporation of the thiosugar in the coronae of the worm nanoparticles results in a change in the balance of the relative core and coronal volumes ultimately changing *p* and hence morphology. However, clear guidelines

cannot be enunciated at this point and we are currently evaluating this in more detail.

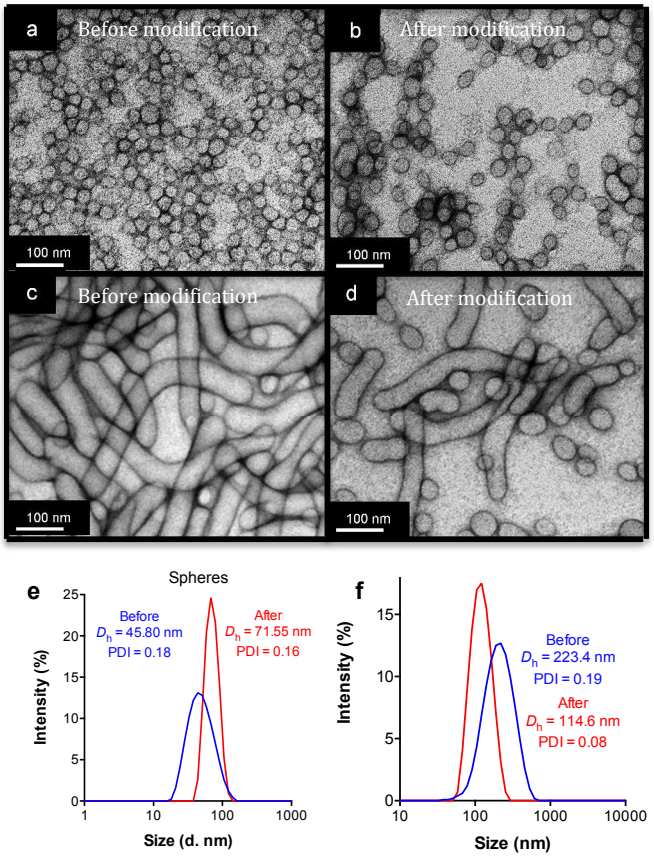

Figure 3. Representative TEM images of (a) p[(DMAEMA$_{29}$-*co*-*t*BAFPEMA$_2$)-*b*-PPMA$_{48}$] before, and (b) after reaction with thio-β-D-glucose tetraacetate; (c) p[(DMAEMA$_{31}$-*co*-tBAFPEMA$_2$)-*b*-PPMA$_{95}$] before modification and (d) after modification with thio-β-D-glucose tetraacetate; (e) and (f) DLS size distributions, hydrodynamic diameters and DLS-polydispersities of the p[(DMAEMA$_{29}$-*co*-*t*BAFPEMA$_2$)-*b*-PPMA$_{48}$] and p[(DMAEMA$_{31}$-*co*-*t*BAFPEMA$_2$)-*b*-PPMA$_{95}$] copolymer before and after modification.

The observed change in morphology is also evident in the DLS data, Fig 3f. Prior to modification the average, 'sphere equivalent', D_h was 223.4 nm with an associated polydispersity of 0.19 whereas after modification the average size drops to 114.6 nm with an associated polydispersity of 0.08.

Conclusions

In summary, we have demonstrated for the first time that Passerini-synthesized PFP-based methacrylic monomers are readily copolymerized with DMAEMA, under homogeneous RAFT conditions, to give novel reactive macro-CTAs that can be employed as the stabilizing solvophilic species in ethanolic RAFTDP formulations with PPMA as a comonomer. Importantly, such formulations yield the full morphological spectrum of soft matter nanoparticles. Reaction of the PFP functionality in the coronal Passerini repeat units with various functional thiols results in the formation of additional novel surface functional species and represents a convenient approach for the generation of new libraries of highly surface modified soft matter nanoobjects.

Notes and references

[a] School of Chemical Engineering, CAMD, UNSW Australia, Kensington, Sydney, NSW 2051, Australia.
[b] Current address: Nanochemistry Research Institute (NRI) and Department of Chemistry, Curtin University, Bentley Campus, Bentley, Perth, WA 6102, Australia.

ABL thanks the Australian Research Council (ARC) for financial support via the Future Fellowship program (FT110100046). PJR also acknowledges the ARC for support via the Discovery Early Career Researcher Award program (DE120101547).

Electronic Supplementary Information (ESI) available: Experimental procedures, FTIR data, additional ^{1}H and ^{19}F NMR spectra See DOI: 10.1039/c000000x/

References

1. J.-T. Sun, C.-Y. Hong and C.-Y. Pan, *Polym. Chem.*, 2013, **4**, 873-881.
2. W.-M. Wan and C.-Y. Pan, *Polym. Chem.*, 2010, **1**, 1475-1484.
3. N. J. Warren and S. P. Armes, *J. Am. Chem. Soc.*, 2014, **136**, 10174-10185.
4. Y. Pei and A. B. Lowe, *Polym. Chem.*, 2014, **5**, 2342-2351.
5. Y. Pei, N. C. Dharsana, J. A. van Hensbergen, R. P. Burford, P. J. Roth and A. B. Lowe, *Soft Matter*, 2014, **10**, 5787-5796.
6. Y. Pei, N. C. Dharsana and A. B. Lowe, *Aust. J. Chem.*, DOI: 10.1072/CH14490.
7. L. A. Fielding, M. J. Derry, V. Ladmiral, J. Rosselgong, A. M. Rodrigues, L. P. D. Ratcliffe, S. Sugihara and S. P. Armes, *Chem. Sci.*, 2013, **4**, 2081-2087.
8. L. Houillot, C. Bui, C. Farcet, C. Moire, J. A. Raust, H. Pasch, M. Save and B. Charleux, *ACS Appl. Mater. Inter.*, 2010, **2**, 434-442.
9. P. J. Roth, T. P. Davis and A. B. Lowe, *Macromol. Rapid Commun.*, 2014, **35**, 813-820.
10. K. Nilles and P. Theato, *J. Polym. Sci., Part A: Polym. Chem.*, 2010, **48**, 3683-3692.
11. Y. Zhu, J. Y. Quek, A. B. Lowe and P. J. Roth, *Macromolecules*, 2013, **46**, 6475-6484.
12. J. Y. Quek, Y. Zhu, P. J. Roth, T. P. Davis and A. B. Lowe, *Macromolecules*, 2013, **46**, 7290-7302.
13. O. Kreye, T. Tóth and M. A. R. Meier, *J. Am. Chem. Soc.*, 2011, **133**, 1790-1792.
14. J. G. Rudick, *J. Polym. Sci., Part A: Polym. Chem.*, 2013, **51**, 3985-3991.
15. S. C. Solleder and M. A. R. Meier, *Angew. Chem. Int. Ed.*, 2014, **53**, 711-714.
16. X.-X. Deng, Y. Cui, F.-S. Du and Z.-C. Li, *Polym. Chem.*, 2014, **5**, 3316-3320.
17. S. Schmidt, M. Koldevitz, J.-M. Noy and P. J. Roth, 2015, **6**, 44-54.
18. J.-M. Noy, M. Koldevitz and P. J. Roth, 2015, **6**, 436-447.
19. A. Blanazs, A. J. Ryan and S. P. Armes, *Macromolecules*, 2012, **45**, 5099-5107.
20. M. Semsarilar, E. R. Jones, A. Blanazs and S. P. Armes, *Adv. Mater.*, 2012, **24**, 3378-3382.
21. D. Zehm, L. P. D. Ratcliffe and S. P. Armes, *Macromolecules*, 2013, **46**, 128-139.